Molecular and Biochemical Characterization of the Parvulin-Type PPIases in *Lotus japonicus*[1[C][W][OA]]

Evangelia D. Kouri, Nikolaos E. Labrou, Spiros D. Garbis, Katerina I. Kalliampakou[2], Catalina Stedel, Maria Dimou, Michael K. Udvardi, Panagiotis Katinakis, and Emmanouil Flemetakis*

Laboratory of Molecular Biology (E.D.K., K.I.K., C.S., M.D., P.K., E.F.) and Laboratory of Enzyme Technology (N.E.L.), Department of Agricultural Biotechnology, Agricultural University of Athens, 11855 Athens, Greece; Center for Basic Research, Biomedical Research Foundation of the Academy of Athens, 11527 Athens, Greece (S.D.G.); and Samuel Roberts Noble Foundation, Plant Biology Division, Ardmore, Oklahoma 73401 (M.K.U.)

The cis/trans isomerization of the peptide bond preceding proline is an intrinsically slow process, although important in many biological processes in both prokaryotes and eukaryotes. In vivo, this isomerization is catalyzed by peptidyl-prolyl cis/trans-isomerases (PPIases). Here, we present the molecular and biochemical characterization of parvulin-type PPIase family members of the model legume *Lotus japonicus*, annotated as LjPar1, LjPar2, and LjPar3. Although LjPar1 and LjPar2 were found to be homologous to PIN1 (Protein Interacting with NIMA)-type parvulins and hPar14 from human, respectively, LjPar3 represents a novel multidomain parvulin, apparently present only in plants, that contains an active carboxyl-terminal sulfurtransferase domain. All *Lotus* parvulins were heterologously expressed and purified from *Escherichia coli*, and purified protein verification measurements used a liquid chromatography-mass spectrometry-based proteomic method. The biochemical characterization of the recombinant *Lotus* parvulins revealed that they possess PPIase activity toward synthetic tetrapeptides, although they exhibited different substrate specificities depending on the amino acid amino terminal to proline. These differences were also studied in a structural context using molecular modeling of the encoded polypeptides. Real-time reverse transcription-polymerase chain reaction revealed that the three parvulin genes of *Lotus* are ubiquitously expressed in all plant organs. LjPar1 was found to be up-regulated during the later stages of nodule development. Subcellular localization of LjPar-enhanced Yellow Fluorescence Protein (eYFP) fusions expressed in Arabidopsis (*Arabidopsis thaliana*) leaf epidermal cells revealed that LjPar1- and LjPar2-eYFP fusions were localized in the cytoplasm and in the nucleus, in contrast to LjPar3-eYFP, which was clearly localized in plastids. Divergent substrate specificities, expression profiles, and subcellular localization indicate that plant parvulin-type PPIases are probably involved in a wide range of biochemical and physiological processes.

Peptidyl-prolyl cis/trans-isomerases (PPIases; EC 5.2.1.8) accelerate the interconversion between prolyl-bond isomers of Pro-containing polypeptide chains, a process that, unaided, is intrinsically slow. PPIases comprise four different families unrelated in their amino acid sequences: the cyclophilins (cyclosporin A-binding proteins); FK506-binding proteins; parvulins, which do not bind immunosuppressants (Fischer and Aumuller, 2003); and the recently identified PPIase, protein phosphatase 2A phosphatase activator (Jordens et al., 2006). All PPIase families are widely distributed in animals, plants, and microorganisms and are found in all major compartments of the cell, implying that these proteins participate in important cellular processes from bacteria to higher eukaryotes (Pemberton and Kay, 2005). Parvulin-like PPIases were identified based on similarity to the prototypical parvulin, EcPar10 of *Escherichia coli* (Rahfeld et al., 1994). Extensively studied members of the parvulin-like PPIases include Ess1/Ptf1 from *Saccharomyces cerevisiae* (Hanes et al., 1989; Hani et al., 1995) and hPin1 (Lu et al., 1996) and hPar14 (Uchida et al., 1999) from human.

Ess1, like human hPin1, consists of two domains, an N-terminal WW domain (InterPro no. IPR001202) and a C-terminal PPIase domain (InterPro no. IPR000297), both being important for the in vivo function of these proteins. The WW domain consists of 35 to 40 amino acid residues and acts as a protein-protein interaction module found in many different proteins (Sudol, 1996). Both Ess1 and hPin1 are characterized as PIN1 (Protein Interacting with NIMA)-type parvulin PPIases, as they preferentially recognize substrates with a phosphorylated Ser or Thr N terminal to Pro residue (Ranganathan

[1] This work was supported by the European Social Fund and the Greek national resources project PYTHAROROAS II (funding of research groups at the Agricultural University of Athens) to E.F.

[2] Present address: Laboratory of Molecular Virology, Hellenic Pasteur Institute, Vasilissis Sofias 127, 11521 Athens, Greece.

* Corresponding author; e-mail mflem@aua.gr.

The author responsible for distribution of materials integral to the findings presented in this article in accordance with the policy described in the Instructions for Authors (www.plantphysiol.org) is: Emmanouil Flemetakis (mflem@aua.gr).

[C] Some figures in this article are displayed in color online but in black and white in the print edition.

[W] The online version of this article contains Web-only data.

[OA] Open Access articles can be viewed online without a subscription.

www.plantphysiol.org/cgi/doi/10.1104/pp.108.132415

et al., 1997; Yaffe et al., 1997). Ess1 is the only yeast PPIase that has been shown to be essential for cell survival (Hanes et al., 1989), in contrast to cyclophilins and FK506-binding proteins, where *S. cerevisiae* knockouts did not exhibit any growth defect (Dolinski et al., 1997). Human hPin1 was shown to be an important mitotic regulator, as depletion or mutations in hPin1 induce premature mitotic entry and mitotic arrest in HeLa cells and *Xenopus* egg extracts (Lu et al., 1996; Patra et al., 1999). In agreement with its role as a mitotic regulator, hPin1 was found to interact with a number of phosphoproteins involved in mitosis, like NIMA (Lu et al., 1996) and Cdc25 (Zhou et al., 2000). In addition to its role in mitosis, hPin1 is involved in p53-mediated control of DNA damage, as hPin1 was shown to be important in the activation of the p53-mediated apoptotic pathway (Zheng et al., 2002). Another parvulin-type PPIase, hPar14, which has been characterized in human, shows 34% identity to hPin1 and, in contrast to hPin1, prefers positively charged amino acids preceding Pro (Uchida et al., 1999). hPar14 lacks the N-terminal WW domain of hPin1 and carries an unstructured N-terminal extension, which is important for localization of hPar14 to the nucleus and its binding to DNA (Surmacz et al., 2002; Reimer et al., 2003).

In contrast to the relatively well-studied parvulins from microorganisms and animals, very little is known about the plant parvulin-type PPIases. Only three plant parvulins have been identified so far, AtPIN1 from Arabidopsis (*Arabidopsis thaliana*; Landrieu et al., 2000), MdPin1 from *Malus domestica* (Yao et al., 2001), and DlPar13 from *Digitalis lanata* (Metzner et al., 2001). A common feature of all three characterized plant parvulins is that they belong to the PIN1-type parvulins, as they prefer substrates with a pSer/pThr residue N terminal to Pro. Furthermore, in contrast to the animal PIN1-type parvulins, they lack the WW domain at the N terminus. Instead, they possess a characteristic four-residue insertion, which could play a role in substrate interactions, as deletion of this insertion renders these enzymes unable to rescue the lethal mitotic phenotype of a temperature-sensitive mutation in the *Ess1* gene of *S. cerevisiae*, similar to a truncated form of hPin1 lacking the WW domain (Metzner et al., 2001; Yao et al., 2001). Interestingly, in silico analysis revealed the presence of additional parvulin-type PPIases in the Arabidopsis genome, although nothing is known about the biochemical properties and substrate specificities of these enzymes (He et al., 2004). Furthermore, the exact biochemical and physiological roles of parvulins in plants remain elusive.

Here, we describe the isolation and biochemical characterization of three parvulin-type PPIases, LjPar1, LjPar2, and LjPar3, from the model legume *Lotus japonicus*. LjPar1 possesses the characteristics of PIN1-type parvulins and shows a high degree of similarity with the previously characterized plant PIN1-type parvulins. LjPar2 is a novel plant parvulin sharing features in common with the human hPar14. Finally, LjPar3 is unique among parvulins characterized until now, with homologs found only in plant genomes. In addition to biochemical characterization of three *Lotus* parvulins, we present here developmental and spatial expression patterns of the corresponding genes and data on the subcellular locations of the proteins.

RESULTS

Identification and Characterization of cDNA Clones Coding for Parvulin-Type PPIases in *L. japonicus*

In order to identify cDNA clones coding for parvulin-type PPIases in *L. japonicus*, a bioinformatics approach was undertaken. In silico homology searches of *L. japonicus* cDNA sequences in The Institute for Genomic Research revealed the presence of two distinct tentative consensus sequences (TC15115 and TC17101) and an independent EST sequence (AW719473). The longest cDNA clones corresponding to the three independent transcripts were obtained and fully sequenced, verifying that the tentative consensus sequences represent naturally occurring transcripts. The full-length cDNA clone corresponding to TC15115 encodes a polypeptide of 122 amino acids with a predicted molecular mass of 13.2 kD and a calculated pI of 9.46. Sequence comparisons with other members of the parvulin-type PPIase family showed that the encoded polypeptide is similar to the eukaryotic PIN1-type parvulins, with 81.5% and 51.7% identity to AtPIN1 and hPin1, respectively. The encoded polypeptide was annotated as LjPar1 (Fig. 1). As is the case for the plant PIN1-type parvulins, LjPar1 is a single-domain protein containing only the PPIase domain (Fig. 2). The full-length cDNA corresponding to TC17101 contains an open reading frame with a length of 145 amino acids with predicted molecular mass and pI of 15.2 kD and 9.54, respectively; it was annotated as LjPar2. Sequence comparison showed that LjPar2 shares a high similarity with hPar14 (51.7%; Fig. 1). In contrast, LjPar2 shares only 34.6% and 26.1% identity with LjPar1 and hPin1, respectively. LjPar2 is also a single-domain protein containing the characteristic PPIase domain, although an N-terminal Lys-rich extension is present, as is reported for hPar14 (Fig. 2). In contrast to the relatively short polypeptides encoded by LjPar1 and LjPar2, the third cDNA clone encoded a longer polypeptide, annotated as LjPar3, comprising 289 amino acids with a predicted molecular mass of 32 kD and a calculated pI of 6.08. Interestingly, the LjPar3 polypeptide has some unique characteristics as it is a multidomain protein containing a central PPIase domain (Fig. 2), which is similar to the respective PPIase domains from bacterial parvulins, showing 30% similarity with the EcPar10 PPIase domain. In addition, LjPar3 contains an N-terminal extension having characteristics of a chloroplast-targeting signal peptide and a C terminal sulfurtransferase domain (Fig. 2).

The phylogenetic relationship of *L. japonicus* parvulin-type PPIases to other functionally characterized or

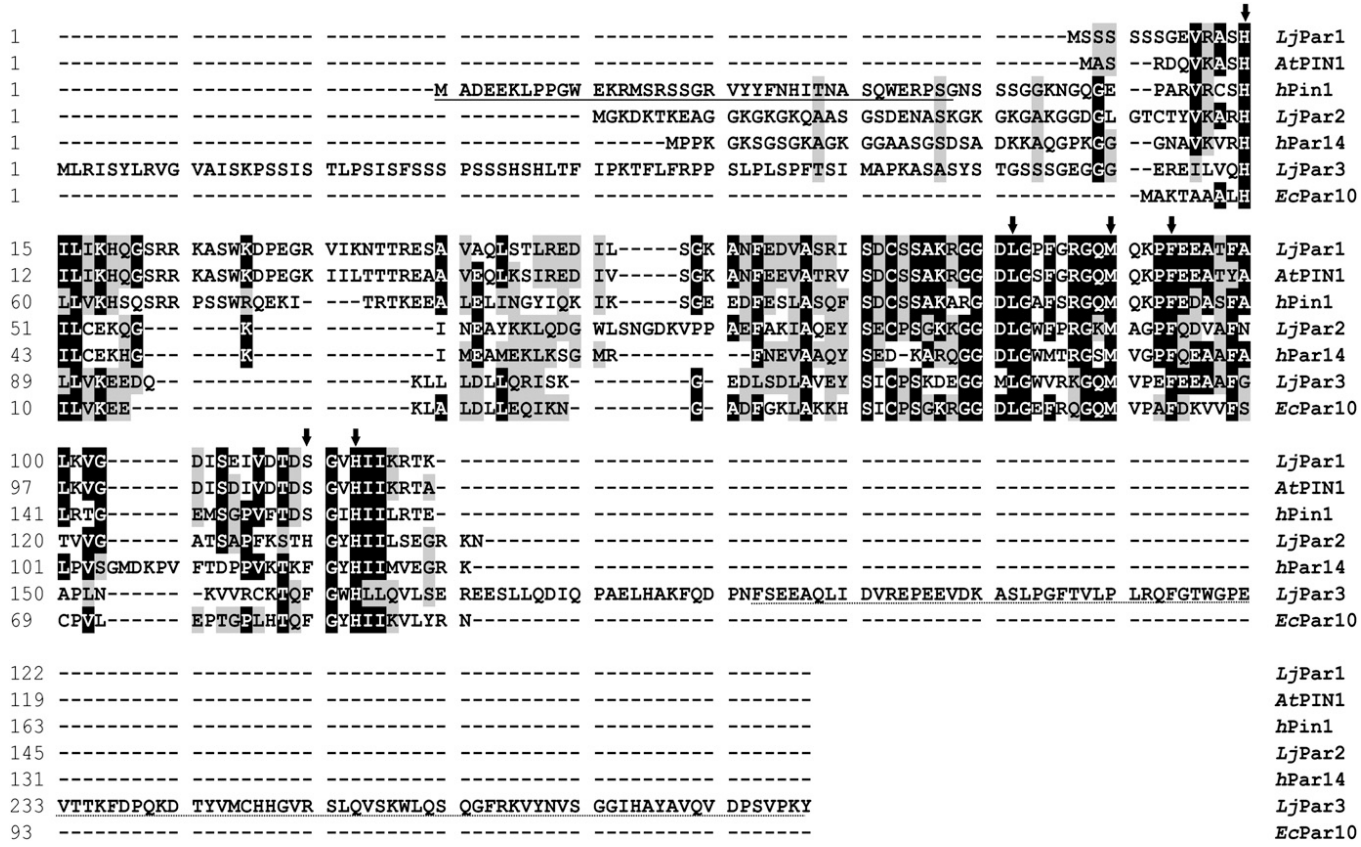

Figure 1. Comparison of the deduced amino acid sequences of *L. japonicus* parvulins with previously characterized members of the parvulin family. Sequences shown include the following: AtPIN1, Arabidopsis PPIase PIN1 (Q9SL42); hPin1, human Pin1 (Q13526); hPar14, human Par14 (Q9Y237); and EcPar10, *E. coli* Par10 (P0A9L5). Identical residues are boxed in black, whereas conservative changes are shown in gray. Dashes represent gaps inserted to maximize the alignment. Sequences were aligned using the ClustalW method with the PAM250 residue weight table followed by manual refinement. Arrows indicate important amino acid residues for the PPIase domain. The WW domain of hPin1 is underlined, and the dashed underline represents the sulfurtransferase domain of LjPar3.

in silico-annotated parvulin-type PPIases was investigated by the construction of a dendrogram generated by multiple amino acid sequence alignment, using the ClustalW method (Fig. 3). The multiple sequence alignment on which the phylogenetic tree is based is given in Supplemental Figure S1. In this phylogenetic tree, *Lotus* parvulins are grouped in three distinct clades. LjPar1 is grouped in the same clade with the previously characterized PIN1-type parvulins from plants and animals, while LjPar2 belongs to the same clade as hPar14. Interestingly, LjPar3 forms a distinct clade with EcPar10 and AtPIN3, a homolog encoded in the Arabidopsis genome.

L. japonicus Parvulins Exhibit PPIase Activities with Differential Substrate Specificities

To determine the catalytic properties of *Lotus* parvulins, the coding sequences of the corresponding cDNAs were subcloned into the pQE-30 vector, which

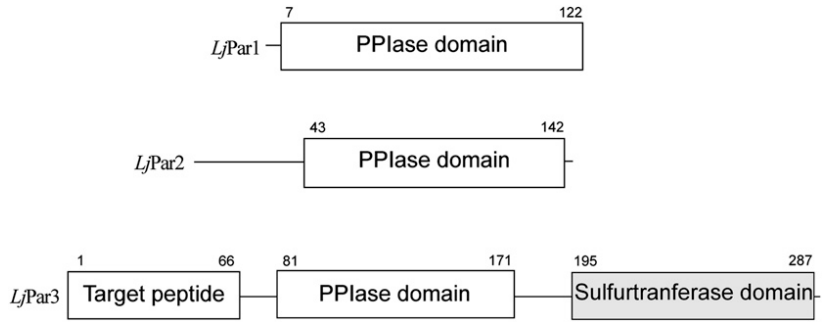

Figure 2. Domain architecture of *L. japonicus* parvulins. The numbers above the boxes denote the amino acid positions of the domains.

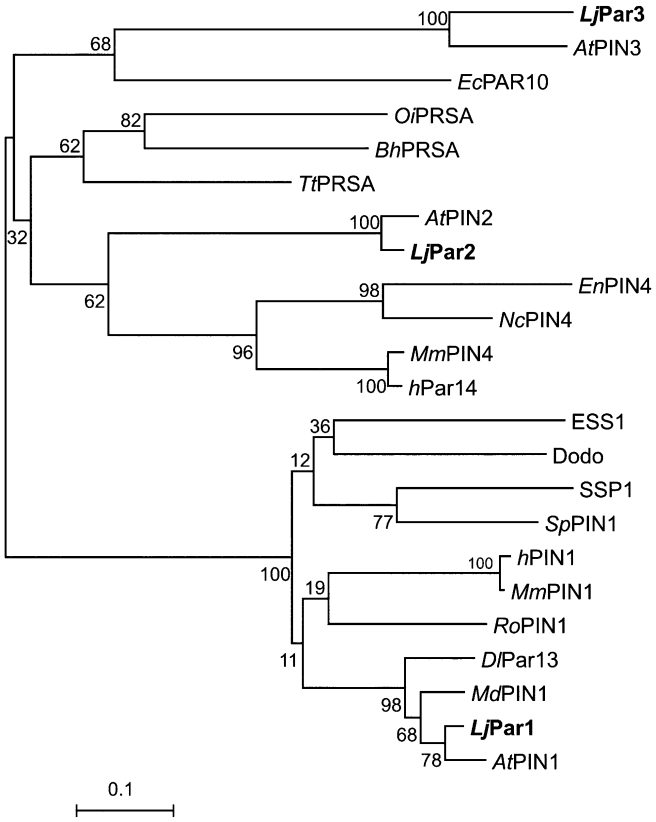

Figure 3. Phylogenetic relationships of LjPar1, LjPar2, and LjPar3 amino acid sequences to other parvulin family members. Full-length amino acid sequences were aligned with the ClustalW program, then manually adjusted to optimize alignment. The neighbor-joining tree was built using MEGA version 4 (Tamura et al., 2007) adopting Poisson correction distance. The tree is drawn to scale, with branch lengths in the same units as those of the evolutionary distances used to infer the phylogenetic tree. The bootstrap values from 1,000 replicates are given at each node. Sequences included are as follows: DlPar13, *D. lanata* PPIase Pin1 (Q9LEK8); MdPIN1, *M. domestica* PPIase Pin1 (Q94G00); AtPIN1, Arabidopsis PPIase Pin1 (Q9SL42); ESS1, *S. cerevisiae* (P22696); SpPIN1, *Schizosaccharomyces pombe* (O74448); SSP1, *Neurospora crassa* (O60045); RoPIN1, *Rhizopus oryzae* parvulin Pin1 (P0C1J8); Dodo, *Drosophila melanogaster* (P54353); MmPIN1, *Mus musculus* (Q9QUR7); hPin1, human (Q13526); EcPar10, *E. coli* (P0A9L5); AtPIN3, Arabidopsis putative PPIase (At5g19370); AtPIN2, Arabidopsis putative PPIase (At1g26550); hPar14, human (Q9Y237); MmPIN4 *M. musculus* (Q9CWW6); EnPIN4, *Emericella nidulans* parvulin Pin4 (Q5B5W1); NcPIN4, *N. crassa* parvulin Pin4 (Q7RYY4); BhPRSA, *Bacillus halodurans* foldase protein prsA precursor (Q9KDN4); OiPRSA, *Oceanobacillus iheyensis* foldase protein prsA precursor (Q8CXK4); TtPRSA *Thermoanaerobacter tengcongensis* foldase protein prsA precursor (Q8R760).

drives the expression of the encoded polypeptide as a C-terminal fusion to a 6xHis tag. For the heterologous expression of LjPar3, the target peptide was removed. The recombinant polypeptides were isolated by nickel-affinity chromatography (Fig. 4, A–C). The purified recombinant parvulins were verified by subjecting the eluates to proteomic analysis with liquid chromatography-mass spectrometry (LC-MS^n). This resulted in the confident identification (>99%) of the three parvulin-type PPIase isoforms (CAM59671.1, CAM59672.1, and CAM59673.1) corresponding to the *L. japonicus* parvulins. No other PPIases were identified. Major surrogate tryptic peptides are shown in annotated form in Figure 4, D to F. The peptide sequence coverage observed ranged from 70.9% to

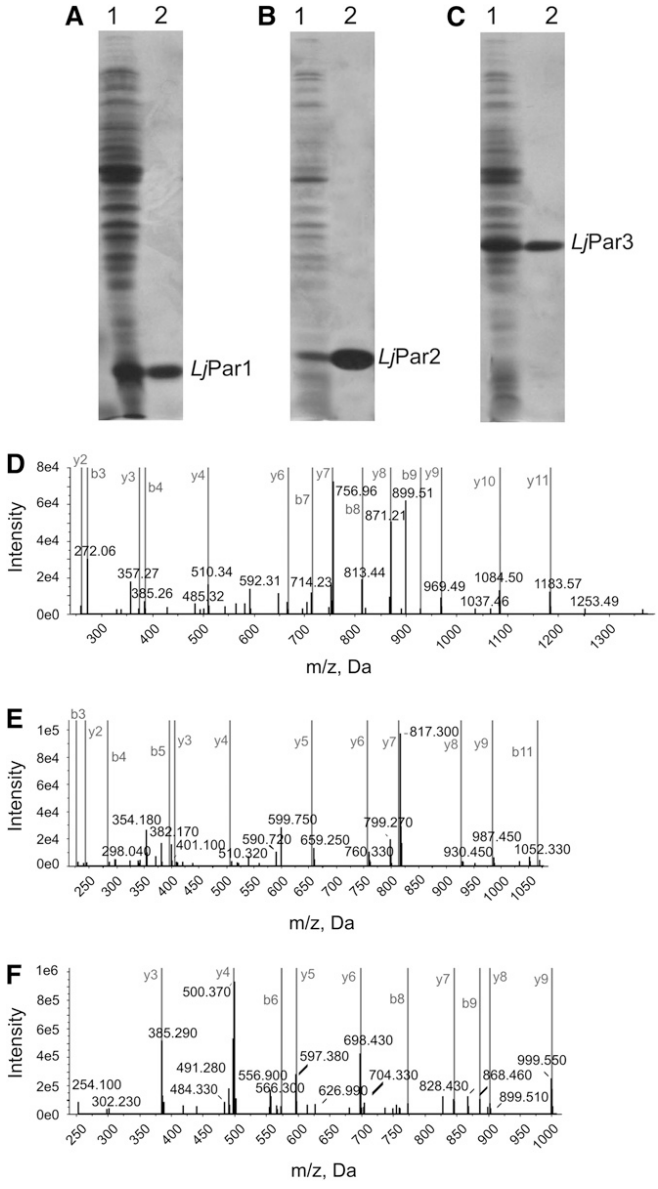

Figure 4. SDS-PAGE and LC-MS^n analysis of the purified recombinant parvulins. A to C, SDS-PAGE analysis of the soluble cytoplasmic protein fraction from elution fractions of *E. coli* M15 [pREP4] cells overexpressing LjPar1 (A), LjPar2 (B), and LjPar3 (C) and the corresponding elution fractions after the purification of the recombinant polypeptides by nickel-affinity chromatography. D, Annotated product ion MS^2 spectrum of the tryptic peptide VGDISEIVDTDSGVHIIK that is uniquely traceable to the LjPar1 protein (CAM59671.1). E, Annotated product ion MS^2 spectrum of the tryptic peptide GGDGLGTCTYVK that is uniquely traceable to the LjPar2 protein (CAM59672.1). F, Annotated product ion MS^2 spectrum of the tryptic peptide ASLPGFTVLPLR that is uniquely traceable to the LjPar3 protein (CAM59673.1).

97.5%. Detailed peptide coverage information is provided in Supplemental Table S1.

The *L. japonicus* recombinant parvulins were tested for PPIase activity on Suc-Ala-Xaa-Pro-Phe-pNA synthetic peptides with the aid of isomer-specific proteolysis using the α-chymotrypsin-coupled assay developed by Fischer et al. (1984). The relative stability of the *Lotus* parvulins toward α-chymotrypsin was tested by the preincubation of the purified enzymes with the amount of the helper protease used in the standard assay. All enzymes were found to be relatively stable against α-chymotrypsin, as no significant loss of activity was detected after a preincubation time of 1 min in the presence of the protease, a time period significant higher than the incubation time used for the determination of the isomerization rate. After a preincubation period of 10 min, we observed 20% and 50% reduction in the activities of LjPar2 and LjPar3, respectively. Due to the limited solubility of nitroaniline peptides, we were unable to determine the individual K_m and V_{max} values; thus, the respective specificity constants were calculated according to Fischer (1994). In order to delineate any differences in the substrate specificity of the three *L. japonicus* parvulins, four alternative residues were tested in the position N terminal to Pro: the nonpolar Ala, the nonpolar aliphatic Leu, the negatively charged Glu, and the positively charged Arg. The results presented in Table I indicated that all *L. japonicus* parvulins exhibit PPIase activity toward synthetic tetrapeptides, although significant differences in specificity were observed, depending on the residue preceding Pro. LjPar1 exhibited a high preference for the tetrapeptide with acidic Glu N terminal to Pro, as k_{cat}/K_m for this peptide was 60-fold and 200-fold higher than for Ala and Leu, respectively. Interestingly LjPar1 had no detectable activity against the tetrapeptide with the positively charged Arg preceding Pro (Table I). For LjPar2, the highest k_{cat}/K_m was detected toward the synthetic peptide containing the aliphatic Leu before Pro, followed by the peptide containing Ala. In contrast to LjPar1, LjPar2 exhibited significant activity against the Arg-Pro bond, while no detectable activity was measured for the Glu-Pro bond (Table I).

Finally, LjPar3 showed high k_{cat}/K_m for most of the tested peptides except the peptide containing the negatively charged Glu before Pro. As with LjPar2, LjPar3 exhibited a small preference toward the synthetic peptide with Leu-Pro and Ala-Pro bonds, while a 2-fold lower value for k_{cat}/K_m was measured for the peptide containing the positively charged Arg (Table I).

LjPar3 Is a Novel Parvulin Containing an Active C-Terminal Sulfurtransferase Domain

As the in vivo substrates for sulfurtransferases have not yet been identified, the enzyme activity of the C-terminal domain of LjPar3 was tested by the formation of SCN^- using thiosulfate or 3-mercaptopyruvate as the donors of the sulfur atom. In agreement with the in silico prediction, the C-terminal domain of LjPar3 was able to transfer a sulfur atom, with a preference for thiosulfate to 3-mercaptopyruvate as the substrate donor. The rate data obtained fitted better to the Hill equation, which was used for the calculation of the respective kinetic parameters. The use of thiosulfate as substrate resulted in a specific activity of 43.4 μmol min^{-1} mg^{-1}, with a K_m of 5.1 mM, V_{max} of 0.047 μmol min^{-1}, and Hill coefficient of 1.9 (Fig. 5A). When 3-mercaptopyruvate was used as the sulfate donor, the sulfurtransferase specific activity was only 0.54 μmol min^{-1} mg^{-1}, with K_m of 10.1 mM, Hill coefficient of 1.5, and V_{max} of 0.029 μmol min^{-1} (Fig. 5B).

Molecular Modeling

The molecular models of LjPar1, LjPar2, and LjPar3 were constructed based on the known crystal structures of parvulins from Arabidopsis (AtPIN1), human Par14, and *E. coli* Par10, respectively. Verify3D analysis and PROSA II profiles of packing, solvent exposure, and stereochemical properties suggested that the final models were of good overall quality. Despite the high sequence divergence between *L. japonicus* parvulins (Fig. 1), overall predicted enzyme structures are fairly similar (Fig. 6, A–C). However, they show distinct differences in helices α1 and α2, in the loop connecting β1 sheet and α1 helix, in the number and arrangement of β-sheets (three in LjPar1 and LjPar2 and two in LjPar3), and in the arrangement of helices α1 and α2. LjPin1 contains a rather extended loop that connects β1 sheet and α1 helix. This is in contrast to LjPar2 and

Table I. *Comparison of the substrate specificity of LjPar1, LjPar2, and LjPar3*

The k_{cat}/K_m values of LjPar1, LjPar2, and LjPar3 were determined with the protease-coupled PPIase assay as described in "Materials and Methods." N.D., Not detected.

Substrate	k_{cat}/K_m		
	LjPar1	LjPar2	LjPar3
		M^{-1} s^{-1}	
Suc-Ala-Ala-Pro-Phe-pNA	4,100 ± 200	25,700 ± 1,100	546,200 ± 50,000
Suc-Ala-Leu-Pro-Phe-pNA	1,320 ± 20	45,000 ± 2,300	600,700 ± 27,300
Suc-Ala-Glu-Pro-Phe-pNA	255,700 ± 11,400	N.D.	1,860 ± 50
Suc-Ala-Arg-Pro-Phe-pNA	N.D.	17,000 ± 1,500	326,700 ± 47,400

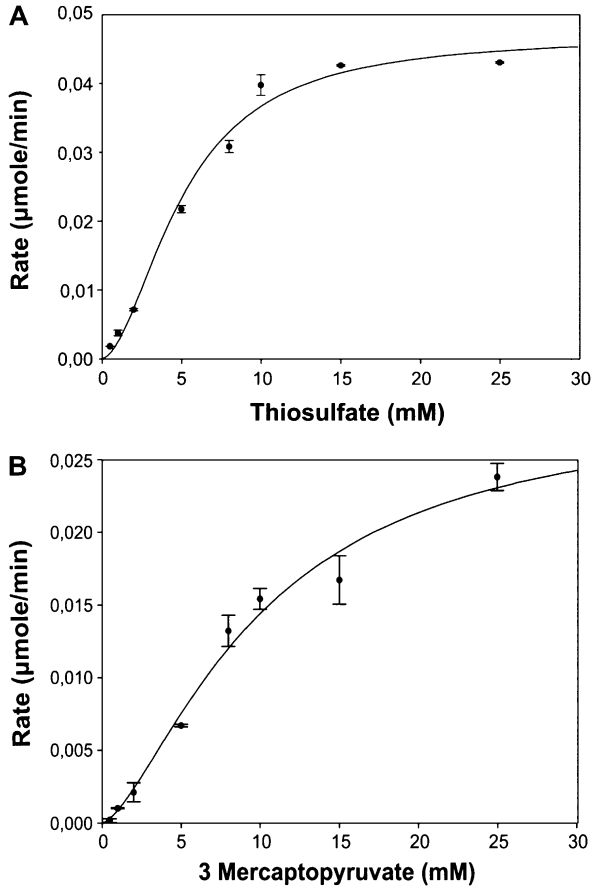

Figure 5. Enzyme activity measurements and kinetic analysis of the recombinant LjPar3 sulfurtransferase domain. Error bars represent SE ($n = 3$).

LjPar3, which possess significantly shorter connecting loops. The first two helices (α1 and α2) form an up-down arrangement in LjPar1 and LjPar2, whereas in LjPar3 they adopt different arrangement. Helix α2 in LjPar1 exhibits a sharp kink and could more accurately be described as two short helices.

Accumulation of Parvulin Transcripts in Symbiotic and Nonsymbiotic Organs of *L. japonicus*

To measure the expression of the three parvulin genes, total RNA was isolated from different *L. japonicus* organs (roots, stems, leaves, flowers, and seed pods) and subjected to reverse transcription and real-time quantitative PCR (RT-qPCR) analysis (Fig. 7). When comparing the expression levels between symbiotic and nonsymbiotic organs, the highest levels of *LjPar1* gene transcripts were detected in mature nodules at 21 d post infection (dpi), while the lowest transcript levels were detected in fully developed flowers (Fig. 7A). In contrast, *LjPar2* transcript levels were found to be more or less constant between the organs tested (Fig. 7A). *LjPar3* transcript levels were very low compared with those of the other two parvulin genes. Our analysis revealed that in mature nodules, *LjPar3* transcript levels were 43-fold and 22-fold lower than those of *LjPar1* and *LjPar2*, respectively. Slightly higher *LjPar3* transcript accumulation was detected in leaves and green seed pods (Fig. 7A).

As parvulins have been implicated in various developmental processes in mammals, we decided to study in more detail their expression pattern during nodule development. We performed RT-qPCR assays on cDNA templates reverse transcribed from total RNA isolated from nodules at 10, 14, 21, and 28 dpi and from whole roots of uninfected 21-d-old plants. Our analysis showed that *LjPar1* transcript levels start to increase in nodules at 21 dpi, where we detected a 1.5-fold increase in comparison with uninfected roots (Fig. 7B). Interestingly, the accumulation of *LjPar1* transcripts continued as nodules grew older and was 2.5-fold higher in nodules at 28 dpi than in roots (Fig. 7B). In contrast, *LjPar2* and *LjPar3* transcripts levels remained similar to those measured in control roots throughout nodule development (Fig. 7B).

Localization of *L. japonicus* Parvulin Gene Transcripts during Nodule Development

Spatial localization of *L. japonicus* parvulin gene expression during nodule development was determined by an RNA-RNA in situ hybridization approach. At 10 dpi, high levels of *LjPar1* transcripts were detected in the nodule inner cortical cells and vascular bundles. Hybridization signal was also visible in both the infected and uninfected cells of the central tissue (Fig. 8A). Similarly, *LjPar2* transcripts were detected throughout the developing nodule, both in the central tissue and in surrounding cortex and vascular bundles (Fig. 8E). Finally, for *LjPar3*, strong hybridization signal was detected in the central tissue, the inner cortical cells, and the connecting vascular bundles. Interestingly, hybridization signal was more intense around the nucleus of the infected and cortical cells (Fig. 8I). In nodules at 14 dpi, *LjPar1* transcript accumulation was observed in the central tissue in both infected and uninfected cells and in the surrounding cortex with the vascular bundles. Interestingly, like *LjPar3*, *LjPar1* transcripts were found to accumulate mainly around the nucleus in all cell types (Fig. 8B). For *LjPar2* hybridization, signal was equally strong in both the central tissue and the surrounding cortical cells. In this case, hybridization signal was equally distributed in the cytoplasm. At 14 dpi, *LjPar3* transcripts continued to accumulate in the infected and uninfected cells, nodule inner cortex, and vascular bundles, with the hybridization signal being more intense around nuclei (Fig. 8J). In mature nodules at 21 dpi, the spatial expression pattern of the *LjPar* genes remained similar to that observed at 14 dpi. *LjPar1* and *LjPar3* transcripts were clearly detected at higher levels around nuclei (Fig. 8, C, M and K, O, respectively). In contrast, the hybridization signal for *LjPar2* remained equally distributed within the cytoplasm (Fig. 8, J and N). During the last developmental stage

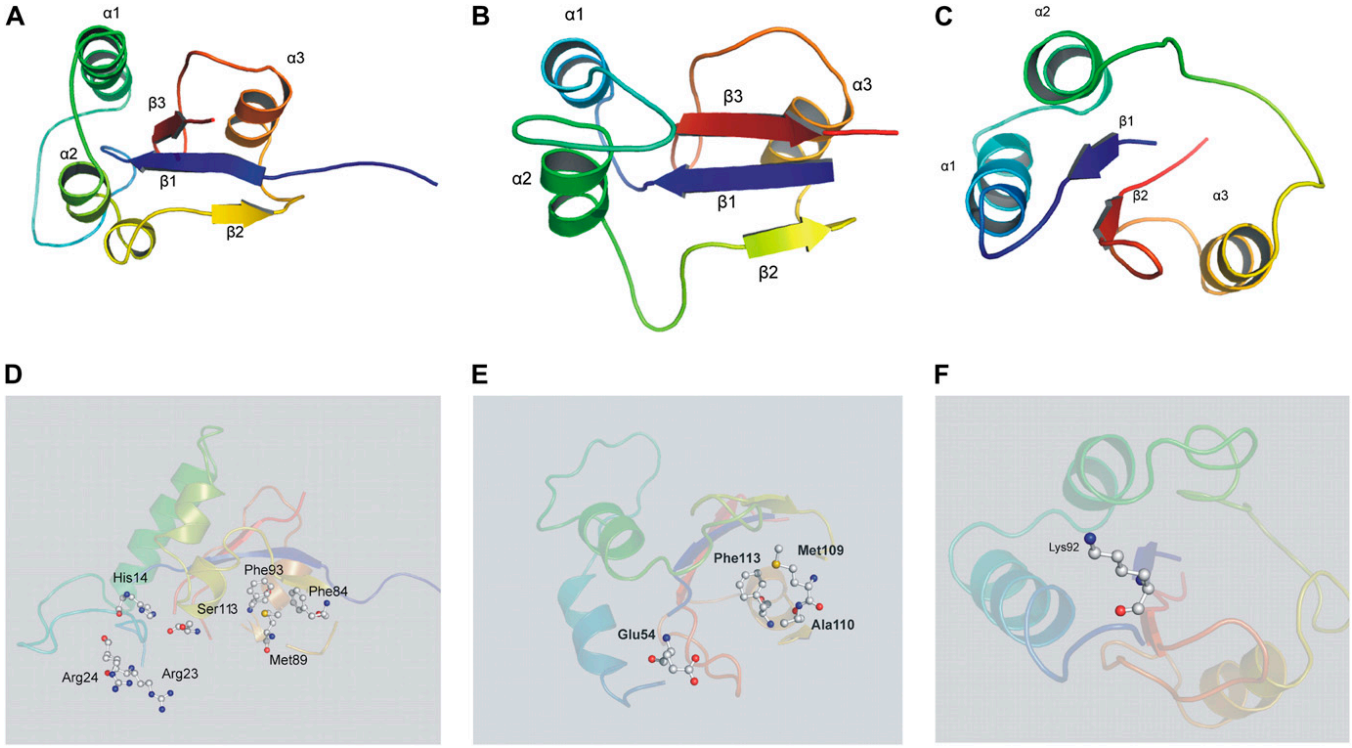

Figure 6. Structural representations of molecular models of *L. japonicus* parvulins and diagrams of a subunit of each enzyme model. A and D, LjPar1. B and E, LjPar2. C and F, LjPar3. Selected residues that are discussed in the text are depicted in a ball-and-stick representation and labeled. [See online article for color version of this figure.]

examined, at 28 dpi, nodules showed clear signs of senescence, including brown color and highly vacuolated infected cells (Fig. 8, D, H, and L). During this late developmental stage, *LjPar1* transcripts were mainly detected in the nodule vascular bundles and inner cortical cells, with staining also being visible in the central tissue and especially around the nuclei (Fig. 8D). For *LjPar2*, the hybridization signal was barely visible, mainly in the nodule vascular bundles and inner cortical cells (Fig. 8H). Finally, *LjPar3* transcripts were mainly observed in the vascular bundles and inner cortex, while in the central tissue the hybridization signal was mainly visible around nuclei (Fig. 8L).

As a negative control, sections of *L. japonicus* nodules at 15 dpi were hybridized with sense digoxigenin-11-rUTP-labeled RNA probe transcribed from the respective cDNA clones. No signal was associated with this probe. Hybridization with *LjPar2* sense RNA is shown (Fig. 8P).

Subcellular Localization of *L. japonicus* Parvulins

In order to probe the subcellular localization of the *L. japonicus* parvulins, we chose to use the transient expression of enhanced Yellow Fluorescence Protein (eYFP) fusions in Arabidopsis epidermal leaves. This decision was dictated by the fact that previous attempts to use fluorescence fusions to study the subcellular localization of polypeptides in *L. japonicus* were hampered by the presence of high levels of autofluorescence in different organs, especially roots and nodules (Simon-Rosin et al., 2003). As the in silico analysis failed to provide direct evidence for the presence of any putative signal sequences in LjPar1 and LjPar2 polypeptides, both C- and N-terminal fusions with eYFP were constructed and tested for any differences in the apparent subcellular localization of the recombinant polypeptides. In the case of LjPar3, the complete open reading frame, containing the putative targeting peptide, was fused to the N terminus of eYFP. For LjPar1, both C- and N-terminal eYFP fusions resulted in comparable localizations, with the recombinant polypeptide accumulating in both the cytoplasm and the nucleus of the epidermal cells. Localization of the LjPar1-eYFP fusion is presented here (Fig. 9A). In the case of the LjPar2-eYFP fusion, the recombinant polypeptide was again localized throughout the cytoplasm and nucleus of the transformed epidermal cells (Fig. 9B). Similarly, transient expression of the eYFP-LjPar2 fusion resulted in identical localization of the recombinant polypeptide (data not shown). Transient expression of the LjPar3-eYFP fusion clearly indicated that the recombinant polypeptide is transported in plastids (Fig. 9C). Plastid localization was confirmed by the localization of chlorophyll autofluorescence (Fig. 9D) and its overlay with the LjPar3-eYFP fluorescence (Fig. 9E). As a control to our localization experiments, we also transformed

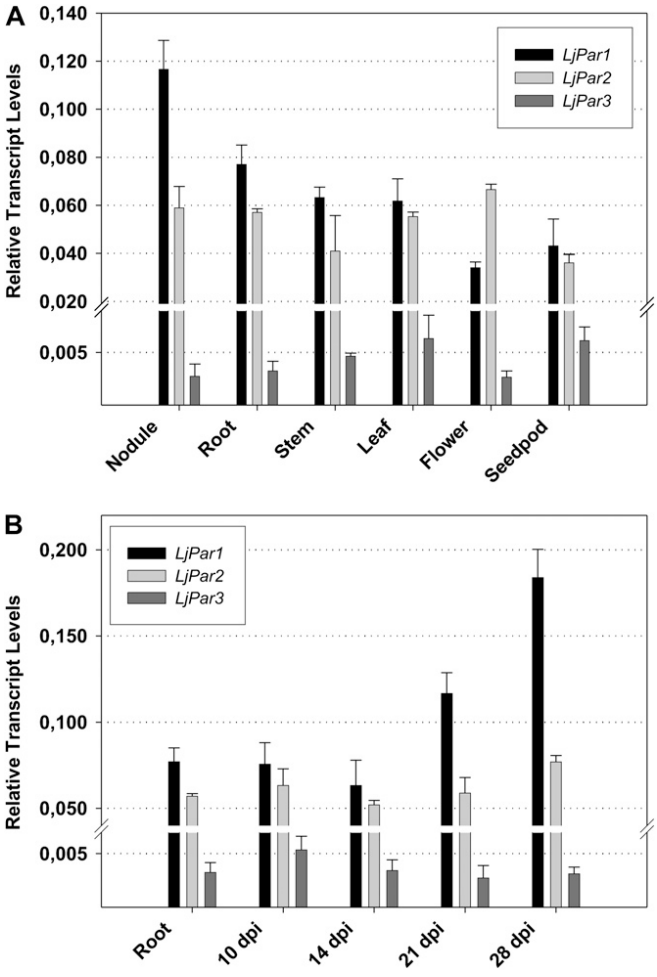

Figure 7. Accumulation of *LjPar1*, *LjPar2*, and *LjPar3* gene transcripts in mature nodules (21 dpi) and nonsymbiotic organs (A) and during various stages of nodule development (B). Total RNA was isolated, and poly(A^+) RNA was reverse transcribed to cDNA and subjected to real-time qPCR using gene-specific primers. Relative mRNA levels were calculated with respect to the levels of the ubiquitin transcripts. Bars show means ± SD ($n = 4$).

Arabidopsis epidermal cells with the parent plasmid, transiently expressing eYFP polypeptide. Consistent with previous observations, eYFP was found to accumulate in the cytoplasm and nucleus (Fig. 9F).

DISCUSSION

L. japonicus Possesses Three Parvulins with Distinct Structural and Biochemical Properties

In this paper, we describe the biochemical and molecular characterization of the parvulin-type PPIase family from *L. japonicus*. Three distinct parvulin-type PPIases were identified in this model species and annotated as LjPar1, LjPar2, and LjPar3. LjPar1 and LjPar2 represent single-domain polypeptides and contain only the main catalytic core of PPIases (InterPro no. IPR000297), as do previously reported homologs in Arabidopsis (Landrieu et al., 2000), *M. domestica* (Yao et al., 2001), and *D. lanata* (Metzner et al., 2001). In contrast, LjPar3 represents a unique multidomain parvulin that contains a functional C-terminal sulfurtransferase/rhodanese-like domain (InterPro no. IPR001763) and an N-terminal plastid target peptide in addition to a central PPIase catalytic domain. Interestingly, our in silico analysis revealed the presence of LjPar3 homologs exclusively in plant genomes. Furthermore, plants are the only organisms possessing representatives of all types of parvulin PPIases.

Our results showed that all *L. japonicus* parvulins exhibit PPIase activity toward synthetic tetrapeptides. Nevertheless, we measured significant differences in the specificity constants of these enzymes toward the different peptides, depending on the side chain properties of the residue preceding Pro (Table I). Molecular models were constructed for the PPIase domains of the three enzymes and used to explore structure-function relationships in the family and to put the kinetics data from the selected peptide substrates into a structural context. LjPar1 contains a catalytic site composed of two components. The first is the anion-binding site that is structurally variable and preferentially recognizes substrates with a negatively charged residue N terminal to Pro. The second component is a site formed by a conserved group of hydrophobic residues located in the C-terminal domain of the polypeptide, which is occupied by the Pro ring of substrate. Examination of conserved residues (Fig. 1) in the context of the model (Fig. 6A), and comparison of the model with PIN1 from Arabidopsis (Landrieu et al., 2002) and human PIN1 (Zhang et al., 2007), crystal structures (where specificity-determining residues are understood) provide a clear explanation for the strong preference of LjPar1 for Glu at the position preceding the substrate Pro. Residues Arg-23 and Arg-24 in LjPar1, located in a $\beta1/\alpha1$ loop region, are well positioned to interact with the substrate and point toward the anion-binding site (Fig. 6D). This is consistent with the kinetic data in Table I, where hydrophobic or positively charged residues at this position in the substrate result in dramatic reduction in catalytic efficiency. This basic cluster is equivalent to those found in AtPIN1 (Arg-21 and Arg-22) and hPin1 (Arg-68 and Arg-69), which are proposed to form the anion-binding site. Three residues, Phe-84, Met-89, and Phe-93, which are conserved in hPin1 and AtPIN1, form a hydrophobic pocket. This pocket is occupied by the pyrrolidine Pro ring of the substrate and forms part of the catalytic domain. Other conserved residues that are located in close spatial proximity to the substrate-binding site are Ser-113 and His-14. Their side chains point toward the anion-binding site and probably contribute to the overall architecture of the pocket and/or to catalysis. This notion is supported by the inability of the His-59→Leu mutant form of hPin1 to support the growth of the yeast *ess1*$^-$ mutant strain (Behrsin et al., 2007).

In the case of LjPar2 (Table I), the enzyme shows moderate preference for positively charged and hy-

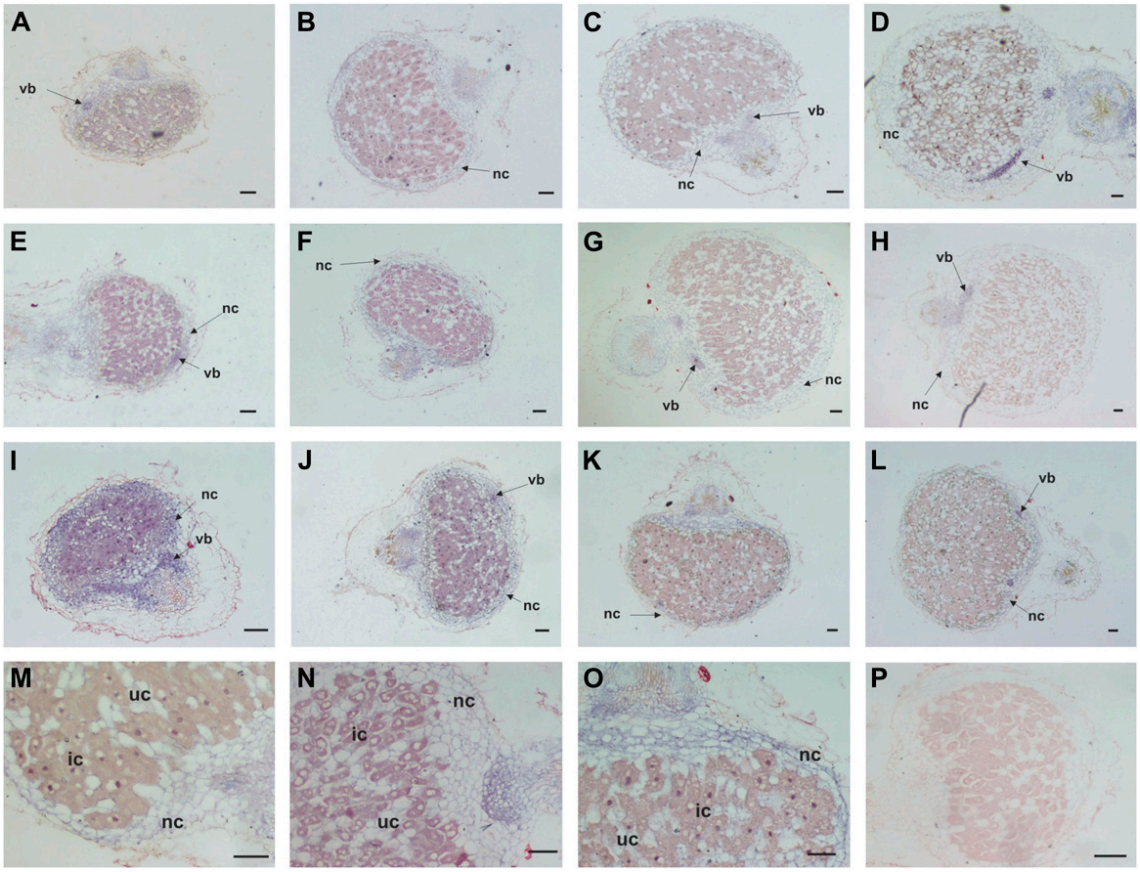

Figure 8. In situ localization of *L. japonicus* parvulin transcripts during nodule development. Hybridization signal is visible as blue-purple precipitate. A to D, Localization of *LjPar1* transcripts in nodules at 10, 15, 21, and 28 dpi, respectively. M, Closeup of a nodule at 21 dpi hybridized with *LjPar1* antisense RNA probe. E to H, Localization of *LjPar2* transcripts in nodules at 10, 15, 21, and 28 dpi, respectively. N, Closeup of a nodule at 21 dpi hybridized with *LjPar2* antisense RNA probe. I to L, Localization of *LjPar3* transcripts in nodules at 10, 15, 21, and 28 dpi, respectively. O, Closeup of a nodule at 21 dpi hybridized with *LjPar3* antisense RNA probe. P, As a negative control, sections were hybridized to sense RNA probe transcribed from the respective cDNA clones. ic, Infected cells; nc, nodule cortex; uc, uninfected cells; vb, vascular bundle. Bars = 100 μm.

drophobic residues at the position preceding the substrate Pro, whereas the enzyme virtually fails to catalyze the reaction with peptide substrate containing Glu at this position. Both sequence alignment and structural models indicate that LjPar2 lacks the positively charged residues (Arg-21 and Arg-22) that determine the substrate specificity of LjPar1. LjPar2 exhibits an entirely different structure in the corresponding region; in particular, the loop between the β1 sheet and the α1 helix is much shorter in LjPar2 than in LjPar1. This suggests that the mechanism determining substrate specificity is quite different between LjPar1 and LjPar2. There is no positively charged residue in this region; however, negative charge is contributed by the side chain of Glu-54. Its side chain points toward the anion-binding site and may be responsible for the enzyme's preference for neutral and positively charged residues preceding the substrate Pro. Comparison of the LjPar2 model with hPar14 indicates that Met-109, Ala-110, and Phe-113 likely form the substrate hydrophobic binding pocket. The Met and Phe residues, but not Ala, are also conserved in EcPar10, hPin1, and AtPIN1. However, Ala-110 is conserved in LjPar2 homologs from other plants.

Residues of the substrate-binding pockets of LjPar1, LjPar2, and LjPar3 are highly conserved. However, LjPar3 lacks the positively charged residues that determine the substrate specificity of LjPar1 and, as in the case of LjPar2, the loop between the β1 sheet and the α1 helix is much shorter. Glu-54 of LjPar2 has been substituted for Lys-92 of LjPar3. Its positive side chain points in an orientation opposite to the binding site; therefore, it does not exclude the binding of positively charged peptides with Arg at the position preceding the substrate Pro.

LjPar3 Is a Unique Multidomain Parvulin Found Only in Plants

As predicted from the deduced amino acid sequence, LjPar3 is a unique multifunctional parvulin containing a C-terminal sulfurtransferase domain.

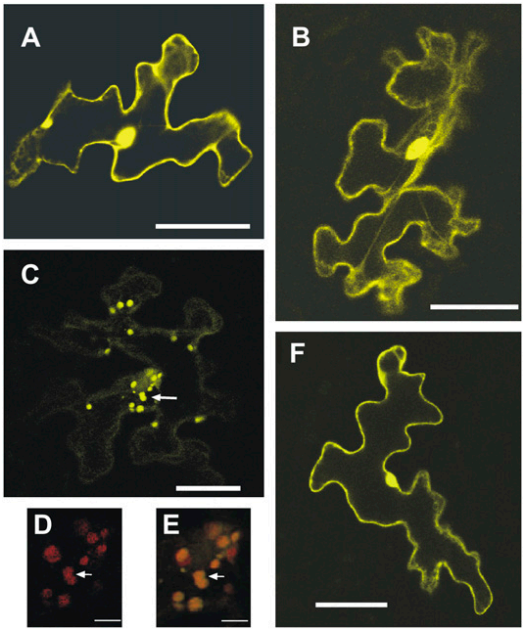

Figure 9. Transient expression of parvulin fusions with eYFP in Arabidopsis leaf epidermal cells. eYFP fluorescence was localized using a laser scanning confocal microscope. A, LjPar1-eYFP recombinant polypeptide was localized in both the cytoplasm and the nucleus of the expressing cells. B, LjPar2-eYFP fusion was localized throughout the cytoplasm and the nucleus. C, LjPar3-eYFP fusion was mainly localized in plastids of the epidermal cells. D and E, Closeups of C showing chlorophyll autofluorescence and the overlay of chlorophyll and eYFP fluorescence, respectively. F, Localization of eYFP polypeptide in epidermal cells. Bars = 40 μm. [See online article for color version of this figure.]

The sulfurtransferase domain is found either in single-domain proteins, in tandem repeats with the C-terminal domain being catalytically active, or in multidomain proteins. Our results demonstrated that the C-terminal extension in the LjPar3 polypeptide is an active sulfurtransferase, able to transfer a sulfur atom from both thiosulfate and 3-mercaptoyruvate to cyanide, although with a clear preference for thiosulfate as a donor molecule. The preference of LjPar3 for thiosulfate is in agreement with previous results showing that the single-domain sulfurtransferases have a high substrate specificity toward thiosulfate, whereas double-domain sulfurtransferases from Arabidopsis show a preference for 3-mercaptopyruvate (Bauer et al., 2004). Thus, the C-terminal domain of LjPar3 belongs to the class of thiosulfate:cyadine sulfurtransferases (EC 2.8.1.1). A common feature of all catalytically active sulfurtransferase domains is the presence of the active site Cys, found in the characteristic motif CXXGX[R/T] forming the active site loop (Cipollone et al., 2007). This Cys residue is present in the corresponding motif CHHGVR found in LjPar3. In addition, the presence of two His residues correlates with the existence of two basic residues in the active site loops of known thiosulfate:cyadine sulfurtransferases, in contrast to the uncharged residues found in the biochemically characterized 3-mercaptopyruvate:cyadine sulfurtransferases (EC 2.8.1.2; Bordo and Bork, 2002). The variability of the residues found in the catalytic loop of known sulfurtransferases possibly reflects variability in their in vivo substrates, as the side chains of these residues define the ridge of the catalytic pocket. To our knowledge, LjPar3 sulfurtransferase active site has a unique amino acid composition among the characterized members of this family, possibly indicating its adaptation to a specific and/or unique in vivo substrate.

L. japonicus Parvulin Genes Are Ubiquitously Expressed and Their Proteins Possibly Fulfill Divergent Physiological Roles

Despite the well-studied roles of parvulin-type PPIases in mammals, very little is known about the possible physiological functions of these enzymes in plants. Noticeably, the only clue about the possible physiological role of parvulins in plants comes from the finding that juglone, a specific inhibitor of the parvulin-type PPIases, is able to inhibit the Aux/IAA-SCF^{TIR1} interaction (Dharmasiri et al., 2003; Tian et al., 2003). This observation indicates the possible involvement of a parvulin-type PPIase in auxin signaling and protein degradation, although further work is needed for the elucidation of the exact molecular mechanism.

During the past years, *L. japonicus* has been widely used as a model legume for the study of nodule organogenesis. Thus, we choose to study the temporal and spatial expression of the parvulin genes during nodule development, as nodule formation is also used as a model organogenesis process. Expression profiling of the parvulin genes revealed that all three genes are expressed in all tissues studied, although the highest transcript levels were found for *LjPar1* in nodules. Interestingly, in developing nodules *LjPar1* transcript levels begin to increase at 21 dpi and continue to increase at 28 dpi. At this later developmental stage, nodules are characterized by morphological changes indicative of senescence, including color change and the presence of vacuoles in the infected cells (Fig. 8D). Nodule senescence is a complex physiological process that is characterized at the molecular level by activation of proteolytic enzymes and an increase in the amount of reactive oxygen species (Puppo et al., 2005). Interestingly, hPin1 has been shown to mediate the accumulation of $p66^{sch}$, which translates oxidative damage in cell death, as it is involved in the production of reactive oxygen species (Pinton et al., 2007). Furthermore, hPin1 is related to many time-dependent functions of mammalian cells like cell growth, genotoxic and other stress responses, immune responses, germ cell development, and neuronal differentiation and survival (Lu et al., 2007). Clearly, much further work is needed to demonstrate the involvement of the homologous plant parvulins in similar cell processes.

Our results on the localization of parvulin-eYFP fusions showed that LjPar1 polypeptide accumulates in both the cytoplasm and nucleus of epidermal cells (Fig. 9, A and B). These results are in agreement with the distribution of DlPar13 PIN-type enzyme activity in subcellular fractions of proembryogenic masses of *D. lanata*, where DlPar13 activity in the cytoplasmic and nucleic fractions represented almost 90% of the total activity. Similar results were obtained by the immunoblotting of DlPar13 in various subcellular fractions from the proembryogenic masses (Metzner et al., 2001). In contrast, hPin1 was found to be almost exclusively localized in the nucleus of HeLa cells (Lu et al., 1996).

Our temporal and spatial transcript analysis revealed that *LjPar2* transcript levels were more or less constant between organs tested, indicating possible housekeeping functions for this parvulin. Furthermore, subcellular localization for LjPar2-eYFP fusions are in agreement with the distribution of the close homolog hPar14 polypeptide, which has been show to accumulate in both the nucleus and the cytoplasm of HeLa cells (Surmacz et al., 2002). An important feature of *LjPar2* is the presence of an unstructural N-terminal extension rich in basic amino acid residues, mainly Lys (Fig. 1). In hPar14, the respective basic N-terminal extension has been shown to be necessary for the nuclear localization of the protein and high-affinity binding to DNA (Surmacz et al., 2002). The results on hPar14 localization together with its structural similarities to the HMGB/HMGN protein family led to the hypothesis that it may be involved in cell cycle regulation and gene transcription. Furthermore, hPar14 association with preribosomal ribonucleoprotein complexes may indicate its involvement in ribosome biogenesis and/or necleolar reassembly of mammalian cells (Fujiyama et al., 2002). However, whether LjPar2 participates in similar cellular processes in plants remains an open question.

One of the most intriguing questions arising from our work is about the exact physiological role of LjPar3, as this multidomain parvulin is unique in plants. Interestingly, LjPar3-eYFP was found to accumulate in the plastids of transformed epidermal cells, in agreement with the in silico prediction of a chloroplast target peptide at the N-terminal end of the protein. Although sulfurtransferases have received increased attention due to their abundance in all life kingdoms, their exact physiological roles are subject to debate, mainly due to the fact that the search for their in vivo substrates remains inconclusive. Proposed functions for sulfurtransferases include cyanide detoxification (Sylvester and Sander, 1990), sulfur and selenium metabolism (Ramirez et al., 2002), and the formation of iron-sulfur clusters in target proteins (Pagani et al., 1984). More is known on the physiological roles of proteins containing sulfurtransferase domains with other characterized protein domains. These include the ThiI- and ThiF/MoeB-related proteins, which are involved in the metabolism of the sulfur-containing thiamin and molybdopterin (Palenchar et al., 2000; Mueller et al., 2001). From the studies on these multidomain proteins, it can be argued that the involvement of the sulfurtransferase domain in a given process is possibly related to the functional properties of the accompanying domain. Taking into account that in LjPar3 the sulfurtransferase domain is coupled to a PPIase domain, it seems plausible that the two domains could act on the same target protein, possibly by assisting the adoption of its native architecture by the simultaneous peptide-prolyl bond isomerization and the transfer of sulfur atoms on specific residues. Identification of the in vivo sulfur donors for LjPar3 remains a task for the future; however, it seems unlikely that this role is fulfilled by thiosulfate or 3-mercaptopyruvate, given the enzyme's low affinity for these substrates in vitro, as the observed values were in the millimolar range.

In conclusion, we have identified and biochemically characterized three parvulin-type PPIases from the model legume *L. japonicus*. To our knowledge, this is the first report of a family-wide study of the plant parvulins. Our results revealed different substrate specificities of the three enzymes, which probably reflect differences in their natural targets in planta. The ubiquitous presence of PPIase in plants, together with the presence of the novel LjPar3 homologs, underscores the importance of prolyl cis/trans isomerization in various biological processes during plant life. Further work needs to be done to clarify the processes that involve PPIase-dependent prolyl cis/trans isomerization in plants. To this end, we plan to use reverse genetics, including TILLING and RNA interference, to ascertain the function of parvulin-type PPIase in *L. japonicus*.

MATERIALS AND METHODS

Plant Material and Growth Conditions

Lotus japonicus (Gifu B-129) seeds were kindly provided by Dr. Jens Stougaard (University of Aarhus, Denmark). The plants were grown in a controlled environment with an 18-h-day/6-h-night cycle, a 22°C/18°C day/night regime, and 70% humidity. Prior to germination, seeds were scarified for 5 min with H_2SO_4, sterilized for 20 min in a solution containing 2% (v/v) NaOCl and 0.02% (v/v) Tween 20, and finally rinsed three times in sterile, distilled water. Seeds were pregerminated at 18°C in the dark for 72 h, and the small plants were grown in B&D nutrient solution (Broughton and Dilworth, 1971). For the inoculation with rhizobia, 72-h seedlings were spot infected with an A_{600} of 0.1 suspension culture of *Mesorhizobium loti* (strain R7A) and the plants were grown in nitrogen-free B&D nutrient solution.

Expression of *L. japonicus* Parvulins in *Escherichia coli* and Purification of the Recombinant Polypeptides

In order to study the catalytic properties of *L. japonicus* parvulins, the coding regions of *LjPar1*, *LjPar2*, and *LjPar3* were amplified from cDNA using the following primers: LjPar1ExF (5′-AAAGAGCTCTCGTCGTCGTCTTCCAGCGGT-3′), LjPar1ExR (5′-AAACTGCAGTTATTTGGTTCTCTTAATAAT-3′), LjPar2ExF (5′-AAAGGATCCGGAAAAGATAAGACAAAGGAG-3′), LjPar2ExR (5′-AAAGAGCTCTCAGTTCTTTCTTCCTTCAGA-3′), LjPar3ExF (5′-AAAGGATCCTCAGCTTCATATAGCACTGGG-3′), and LjPar3ExR (5′-AAAGTCGACTCAGTACTTGGGGACTGATGG-3′). The PCR products were subcloned into the pQE-30 expression vector (Qiagen). For LjPar3, the target peptide was removed. The expression constructs were transformed

in *E. coli* strain M15 [pREP4]. After growth at 37°C to an A_{600} of 0.6 in Luria-Bertani medium containing ampicillin (100 μg mL^{-1}) and kanamycin (25 μg mL^{-1}), expression of the recombinant polypeptides was induced by the addition of 0.5 mM isopropylthio-β-galactoside and the growth of cultures was continued for 5 h at 37°C. Recombinant polypeptides were purified under native conditions by nickel-affinity chromatography (Qiagen) according to the manufacturer's instructions for His-tagged proteins.

LC-MS Proteomic Analysis

The chemical reagents acetonitrile (ACN), ethanol, isopropanol, methanol, acetone, and formic acid (HPLC grade) were obtained from Sigma. Trypsin was proteomics grade (Roche). The ultrapure HPLC-grade water, utilized for LC-MS analysis procedures, was generated from the Barnstead water filtration system. The proteins were reduced by the addition of 2 μL of 50 mM Tris-2-carboxymethyl phosphine (Applied Biosystems) followed by incubation for 1 h at 60°C. The Cys residues were blocked by the addition of 1 μL of 200 mM methyl methanethiosulfonate (MMTS; Applied Biosystems) in isopropanol and 10 min of incubation at room temperature. For the trypsin digestion, 6 μL of freshly prepared trypsin solution (500 ng μL^{-1}) and 16 μL of ultrapure water were added into the protein sample that was then incubated for 12 h at 37°C. Trypsinization was halted with centrifugal lyophilization under vacuum. All LC-MS analyses were performed with the Agilent 6330 Ion Trap MSD system retrofitted to an Agilent 1200 nano-LC system equipped with a microwell plate autosampler. Prior to sample analyses, the Ion Trap MSD system instrument was externally tuned and calibrated using a manufacturer's standard solution. A 3-μL volume from each tryptic peptide sample (reconstituted in 2% ACN and 0.5% formic acid) was injected and then eluted onto a custom-prepared 0.075- × 200-mm reverse-phase capillary column (Zorbax C18; 300-Å pore, 1.8-μm particle; Agilent Technologies) retrofitted onto the nanoelectrospray source (Agilent Technologies) and connected to a 1P-4P-coated, 8-μm tip × 360-μm o.d. × 75-μm i.d. PicoTip nanoelectrospray emitter (New Objective). The mobile phase used an initial isocratic condition for 30 min with mobile phase A at a flow rate of 200 nL min^{-1} in order to load the entire injection volume into the column. To assist this process, an automatic delay volume reduction scheme was enabled for the autosampler module at a sample flush-out factor of 4.0. Peptides were eluted into the MS system with a binary gradient (200 nL min^{-1}) from 100% mobile phase A to 70% mobile phase B (98% ACN and 0.5% formic acid) over 110 min, then 70% to 100% mobile phase B in 20 min, and held at mobile phase B for an additional 10 min. The total duration of the LC run was 200 min, including sample loading, peptide elution, and column reequilibration. Typically, a minimum 70% peptide coverage was achieved for the proteins of interest. Protein identification was performed with the Protein Pilot software program revision 2.0.1 (Applied Biosystems) using both Paragon and Mascot search algorithms (Shilov et al., 2008). The data analysis parameters were as follows: sample type, Cys alkylation, MMTS; digestion, trypsin; instrument, ESI-Trap; custom database, *Lotus japonicus*.

PPIase Activity Assay

Determination of the PPIase activity of recombinant *L. japonicus* parvulins was performed as described previously by Fischer et al. (1984). The assay was conducted as follows. A 1-mL reaction mixture containing 0.45 mg mL^{-1} α-chymotrypsin and recombinant parvulin (10 μg per assay) in 50 mM HEPES and 100 mM NaCl, pH 8.0, was prechilled to 10°C and then rapidly mixed into a cuvette containing the substrate *N*-succinyl-Ala-Xaa-Pro-Phe-*p*-nitroanilide (where Xaa = Ala, Leu, Glu, or Arg). The peptide derivatives were dissolved at a stock concentration of 5 mM in 470 mM LiCl/trifluoroethanol (Kofron et al., 1991). The specificity constants k_{cat}/K_m were determined using the equation $k_{cat}/K_m = (k_b - k_u)/[E]$, where k_b is the first-order rate constant of the PPIase-catalyzed reaction, k_u is the constant of the PPIase-uncatalyzed reaction, and [E] is the PPIase concentration in the assay, assuming that the entire amount of pure enzyme at total concentration represents catalytically active molecules (Fischer, 1994). Substrate concentrations tested were 2.5 to 250 μM in order to verify that [S] $< K_m$ was used for the PPIase reaction (Fischer, 1994). The relative stability of *Lotus* parvulins toward α-chymotrypsin was tested by the preincubation of the purified polypeptides with the amount of α-chymotrypsin used in the standard assay reaction (0.45 mg mL^{-1}) prior to the addition of the peptide substrate and the measurement for PPIase activity. Incubation times ranging from 1 to 10 min were tested. All measurements were made in triplicate.

Sulfurtransferase Assay

The purified recombinant LjPar3 was tested for sulfurtransferase activity against thiosulfate and 3-mercaptopyruvate as the sulfur donors. The activity was determined by measuring the SCN^- formation as the red complex $Fe(SCN)_3$ from cyanide and thiosulfate or 3-mercaptopyruvate (Westley, 1981). The 1-mL assay mixture contained 0.1 M Tris-HCl, pH 9.0, 5 mM KCN, 5 mM mercaptoethanol, and recombinant LjPar3. The reaction was initiated by the addition of $Na_2S_2O_3$ or 3-mercaptopyruvate. After incubation at 37°C for 5, 10, or 20 min, the reaction was stopped by the addition of 200 μL $FeCl_3$ in 13% (v/v) HNO_3. The absorption was read at 460 nm. Measurements were made in triplicate. Reaction product was quantified using a standard curve done with NaSCN standard solution.

Molecular Modeling

The meta-server (Douguet and Labesse, 2001) was used to screen structure databases aiming to find a compatible fold for LjPar1, LjPar2, and LjPar3. Sequences homologous to *Lotus* parvulins were sought in PDB (Berman et al., 2000) using BLAST. The resulting sequence set was aligned with ClustalW. Threading experiments were also carried out using several Web servers, such as Jpred2, the secondary structure prediction server 3D-PSSM (Cuff et al., 1998), a threader using one-dimensional and three-dimensional sequence profiles coupled with secondary structure and solvation potential information (Kelley et al., 2000), and mGenThreader, a multiple sequence profile-based threader (Jones, 1999). A threader, FUGUE (Shi et al., 2001), searching the HOMSTRAD profile database (Mizuguchi et al., 1998), was also employed. The best alignment was then directly submitted to TITO (Labesse and Mornon, 1998) to analyze and validate the chosen structure-sequence alignments. Template secondary structures were automatically assigned during TITO processing. Modeling of *Lotus* parvulins was carried out with MODELLER 6 (Sali and Blundell, 1993). For LjPar1, modeling was based on the structure of PIN1 from Arabidopsis (*Arabidopsis thaliana*; PDB code 1j6yA; Landrieu et al., 2002) as template. For LjPar2, modeling was based on the structure of hPar14 (PDB code 1eq3; Sekerina et al., 2000) as template. For LjPar3, modeling was based on the structure of *E. coli* Par10 (PDB code 1jns; Kuhlewein et al., 2004) as template. In the case of LjPar3, only the PPIase domain was modeled, since all servers failed to find a compatible fold for the sulfurtransferase domain. A rigorous iterative modeling scheme was employed in which four models were constructed and analyzed for each variant alignment. These models were analyzed with Verify3D (Eisenberg et al., 1997) and PROSA II (Sippl, 1993) for packing and solvent exposure characteristics. Model regions corresponding to positive PROSA II profile peaks were treated as possibly resulting from misalignments. Alterations in alignments were tested for these regions. When no further improvements were possible, the model with the best PROSA II score was considered as the final model.

Determination of Transcript Levels Using RT-qPCR Assay

Total RNA was isolated according to standard protocols (Brusslan and Tobin, 1992) and quantified by spectrophotometry and agarose gel electrophoresis. Prior to RT-PCR, the total RNA samples were treated with DNase I (Promega) at 37°C for 45 min. First-strand cDNA was reverse transcribed from 2 μg of DNase-treated total RNA using SuperScript II reverse transcriptase (Invitrogen). PCR fragments were amplified using the following gene-specific primers designed from the transcribed region of each gene using Primer Express 1.5 software (Applied Biosystems): LjPar1F (5′-TCAGTACCCTCCGTGAGGACAT-3′), LjPar1R (5′-TGCAATCGGAGATGCGAGA-3′), LjPar2F (5′-AAAGTCCCCCCAGCAGAGTTT-3′), LjPar2R (5′-CCACCCTTCTTTCCTGATGGA-3′), LjPar3F (5′-GTCCAAGTGGTTGCAGTCACAG-3′), and LjPar3R (5′-GCATGGATTCCCCCAGAA A-3′). Quantitative RT-PCR was performed on the ABI PRISM 7900HT Sequence Detection System using SYBR Green master mix (Applied Biosystems). PCR cycling started with the initial polymerase activation at 95°C for 10 min, followed by 40 cycles of 95°C for 15 s and 60°C for 1 min. Primer specificity and the formation of primers-dimers were monitored by dissociation curve analysis and agarose gel electrophoresis on a 4% (w/v) gel. The expression level of a *L. japonicus* ubiquitin gene was employed as an internal standard for normalization of transcripts using the primers LjUBQF (5′-TTCACCTTGTGCTCCGTCTTC-3′) and LjUBQR (5′-ACCACCAGCACACACACAGACAATCC-3′). For the relative quantification of gene expression, a modification of the comparative threshold

cycle method was used. Relative transcript levels of the gene of interest (X) were calculated as a ratio to the ubiquitin gene transcripts (U) as $(1 + E)^{-\Delta Ct}$, where ΔC_t was calculated as $(C_t^X - C_t^U)$. PCR efficiency (E) for each amplicon was calculated employing the linear regression method on the log(fluorescence) per cycle number data.

In Situ Hybridization

In situ hybridization experiments were performed as described previously (Flemetakis et al., 2000). *L. japonicus* nodules were fixed in 4% (w/v) paraformaldehyde supplemented with 0.25% (v/v) glutaraldehyde in 10 mM sodium phosphate buffer (pH 7.4). Fixed nodules were block stained in 0.5% (w/v) safranin, dehydrated through an ethanol series, and embedded in paraffin, and 8- to 10-μm-thin sections were cut. Antisense and sense RNA probes labeled with digoxigenin-11-rUTP (Roche) were transcribed from the respective cDNA clones using the appropriate RNA polymerase promoters on the plasmid vectors. The probes were partially degraded to an average length of 150 nucleotides. Sections were hybridized overnight at 42°C in 50% (v/v) formamide, 300 mM NaCl, 10 mM Tris-HCl, pH 7.5, 1 mM EDTA, 0.02% (w/v) Ficoll, 0.02% (w/v) polyvinylpyrrolidone, 0.025% (w/v) bovine serum albumin, 10% (v/v) dextran sulfate, and 60 mM dithiothreitol. Hybridization signals were visualized with anti-digoxigenin antibodies conjugated with alkaline phosphatase. Images were processed and prepared for presentation with Photoshop 7 software (Adobe Systems).

Particle Bombardment and GFP Imaging

In order to study the intracellular localization of *L. japonicus* parvulins, fusions with eYFP were transiently expressed in Arabidopsis leaf epidermal cells. The coding regions of *LjPar1*, *LjPar2*, and *LjPar3* were amplified using the restriction sites containing primers LjPar1N-F (5′-AAAAAGATC-TATCATGTCGTCGTCGTC T-3′), LjPar1N-R (5′-GTTAGATCTTTTGGTTC-TCTTAAT-3′), LjPar1C-F (5′-CATTCCATGGCTTCGTCGTCGTCTTCC-3′), LjPar1C-R (5′-GCTGCCCATGGCTTTGGTTCTCTTAAT-3′), LjPar2N-F (5′-CGCGGATCCATGGGAAAAGATAAG-3′), LjPar2N-R (5′-CGCGGA-TCCGTTCTTTCTTCCTTC-3′), LjPar2C-F (5′-CATTCCATGGGAAAAGAT-AAG-3′), LjPar2C-R (5′-GCTGCCATGGCGTTCTTTCTTCCTTC-3′), LjPar3C-F (5′-AAATCATGATCTTGAGAATTTCTTAT-3′), and LjPar3C-R (5′-TTTTC-ATGACGTACTTGGGGACTGA-3′). Amplified fragments were cloned into the respective restriction sites of the pAVA554 plasmid vector, which drives transient expression of the cloned sequences under the control of the double cauliflower mosaic virus 35S promoter.

Microprojectile bombardment of Arabidopsis ecotype Columbia young rosette leaves was performed using a Bio-Rad PDS-1000 biolistic system. Imaging of eYFP and chlorophyll fluorescence was performed using a TCS SP confocal scanner together with a DMR microscope (Leica) 6 to 24 h after bombardment. The excitation wavelength of eYFP and chlorophyll was 488 nm.

Sequence data from this article can be found in the GenBank/EMBL data libraries under accession numbers AM503586 (*LjPar1*), AM503587 (*LjPar2*), and AM503588 (*LjPar3*).

Supplemental Data

The following materials are available in the online version of this article.

Supplemental Figure S1. Multiple sequence alignment of parvulin-type PPIases from various organisms used for the construction of the phylogenetic tree.

Supplemental Table S1. Peptide coverage of the purified recombinant *Lotus* parvulins.

Received November 11, 2008; accepted April 26, 2009; published April 29, 2009.

LITERATURE CITED

Bauer M, Dietrich C, Nowak K, Sierralta WD, Papenbrock J (2004) Intracellular localization of Arabidopsis sulfurtransferases. Plant Physiol **135:** 916–926

Behrsin CD, Bailey ML, Bateman KS, Hamilton KS, Wahl LM, Brandl CJ, Shilton BH, Litchfield DW (2007) Functionally important residues in the peptidyl-prolyl isomerase Pin1 revealed by unigenic evolution. J Mol Biol **365:** 1143–1162

Berman HM, Westbrook J, Feng Z, Gilliland G, Bhat TN, Weissig H, Shindyalov IN, Bourne PE (2000) The Protein Data Bank. Nucleic Acids Res **28:** 235–242

Bordo D, Bork P (2002) The rhodanese/Cdc25 phosphatase superfamily: sequence-structure-function relations. EMBO Rep **3:** 741–746

Broughton WJ, Dilworth MJ (1971) Control of leghaemoglobin synthesis in snake beans. Biochem J **125:** 1075–1080

Brusslan JA, Tobin EM (1992) Light-independent developmental regulation of Cab gene-expression in *Arabidopsis thaliana* seedlings. Proc Natl Acad Sci USA **89:** 7791–7795

Cipollone R, Ascenzi P, Visca P (2007) Common themes and variations in the rhodanese superfamily. IUBMB Life **59:** 51–59

Cuff JA, Clamp ME, Siddiqui AS, Finlay M, Barton GJ (1998) JPred: a consensus secondary structure prediction server. Bioinformatics **14:** 892–893

Dharmasiri N, Dharmasiri S, Jones AM, Estelle M (2003) Auxin action in a cell-free system. Curr Biol **13:** 1418–1422

Dolinski K, Muir S, Cardenas M, Heitman J (1997) All cyclophilins and FK506 binding proteins are, individually and collectively, dispensable for viability in *Saccharomyces cerevisiae*. Proc Natl Acad Sci USA **94:** 13093–13098

Douguet D, Labesse G (2001) Easier threading through Web-based comparisons and cross-validations. Bioinformatics **17:** 752–753

Eisenberg D, Luthy R, Bowie JU (1997) VERIFY3D: assessment of protein models with three-dimensional profiles. Methods Enzymol **277:** 396–404

Fischer G (1994) Peptidyl-prolyl *cis/trans* isomerases and their effectors. Angew Chem Int Ed Engl **33:** 1415–1436

Fischer G, Aumuller T (2003) Regulation of peptide bond *cis/trans* isomerization by enzyme catalysis and its implication in physiological processes. Rev Physiol Biochem Pharmacol **148:** 105–150

Fischer G, Bang H, Mech C (1984) Determination of enzymatic catalysis for the *cis-trans*-isomerization of peptide binding in proline-containing peptides. Biomed Biochim Acta **43:** 1101–1111

Flemetakis E, Kavroulakis N, Quaedvlieg NE, Spaink HP, Dimou M, Roussis A, Katinakis P (2000) *Lotus japonicus* contains two distinct ENOD40 genes that are expressed in symbiotic, nonsymbiotic, and embryonic tissues. Mol Plant Microbe Interact **13:** 987–994

Fujiyama S, Yanagida M, Hayano T, Miura Y, Isobe T, Takahashi N (2002) Isolation and proteomic characterization of human parvulin-associating preribosomal ribonucleoprotein complexes. J Biol Chem **277:** 23773–23780

Hanes SD, Shank PR, Bostian KA (1989) Sequence and mutational analysis of ESS1, a gene essential for growth in *Saccharomyces cerevisiae*. Yeast **5:** 55–72

Hani J, Stumpf G, Domdey H (1995) PTF1 encodes an essential protein in *Saccharomyces cerevisiae*, which shows strong homology with a new putative family of PPIases. FEBS Lett **365:** 198–202

He Z, Li L, Luan S (2004) Immunophilins and parvulins: superfamily of peptidyl prolyl isomerases in Arabidopsis. Plant Physiol **134:** 1248–1267

Jones DT (1999) GenTHREADER: an efficient and reliable protein fold recognition method for genomic sequences. J Mol Biol **287:** 797–815

Jordens J, Janssens V, Longin S, Stevens I, Martens E, Bultynck G, Engelborghs Y, Lescrinier E, Waelkens E, Goris J, et al (2006) The protein phosphatase 2A phosphatase activator is a novel peptidyl-prolyl *cis/trans*-isomerase. J Biol Chem **281:** 6349–6357

Kelley LA, MacCallum RM, Sternberg MJE (2000) Enhanced genome annotation using structural profiles in the program 3D-PSSM. J Mol Biol **299:** 499–520

Kofron JL, Kuzmic P, Kishore V, Colon-Bonilla E, Rich DH (1991) Determination of kinetic constants for peptidyl prolyl *cis-trans* isomerases by an improved spectrophotometric assay. Biochemistry **30:** 6127–6134

Kuhlewein A, Voll G, Hernandez AB, Kessler H, Fischer G, Rahfeld JU, Gemmecker G (2004) Solution structure of *Escherichia coli* Par10: the prototypic member of the parvulin family of peptidyl-prolyl *cis/trans* isomerases. Protein Sci **13:** 2378–2387

Labesse G, Mornon JP (1998) Incremental threading optimization (TITO) to help alignment and modelling of remote homologues. Bioinformatics **14:** 206–211

Landrieu I, De VL, Fruchart JS, Odaert B, Casteels P, Portetelle D, Van MM, Inze D, Lippens G (2000) The *Arabidopsis thaliana* PIN1At gene encodes a single-domain phosphorylation-dependent peptidyl prolyl *cis/trans* isomerase. J Biol Chem **275:** 10577–10581

Landrieu I, Wieruszeski JM, Wintjens R, Inze D, Lippens G (2002) Solution structure of the single-domain prolyl cis/trans isomerase PIN1At from *Arabidopsis thaliana*. J Mol Biol **320:** 321–332

Lu KP, Finn G, Lee TH, Nicholson LK (2007) Prolyl cis-trans isomerization as a molecular timer. Nat Chem Biol **3:** 619–629

Lu KP, Hanes SD, Hunter T (1996) A human peptidyl-prolyl isomerase essential for regulation of mitosis. Nature **380:** 544–547

Metzner M, Stoller G, Rucknagel KP, Lu KP, Fischer G, Luckner M, Kullertz G (2001) Functional replacement of the essential ESS1 in yeast by the plant parvulin *Dl*Par13. J Biol Chem **276:** 13524–13529

Mizuguchi K, Deane CM, Blundell TL, Overington JP (1998) HOMSTRAD: a database of protein structure alignments for homologous families. Protein Sci **7:** 2469–2471

Mueller EG, Palenchar PM, Buck CJ (2001) The role of the cysteine residues of ThiI in the generation of 4-thiouridine in tRNA. J Biol Chem **276:** 33588–33595

Pagani S, Bonomi F, Cerletti P (1984) Enzymic-synthesis of the iron-sulfur cluster of spinach ferredoxin. Eur J Biochem **142:** 361–366

Palenchar PM, Buck CJ, Cheng H, Larson TJ, Mueller EG (2000) Evidence that ThiI, an enzyme shared between thiamin and 4-thiouridine biosynthesis, may be a sulfurtransferase that proceeds through a persulfide intermediate. J Biol Chem **275:** 8283–8286

Patra D, Wang SX, Kumagai A, Dunphy WG (1999) The Xenopus Suc1/Cks protein promotes the phosphorylation of G(2)/M regulators. J Biol Chem **274:** 36839–36842

Pemberton TJ, Kay JE (2005) Identification and comparative analysis of the peptidyl-prolyl cis/trans isomerase repertoires of *H. sapiens*, *D. melanogaster*, *C. elegans*, *S. cerevisiae* & *Sz. pombe*. Comp Funct Genomics **6:** 277–300

Pinton P, Rimessi A, Marchi S, Orsini F, Migliaccio E, Giorgio M, Contursi C, Minucci S, Mantovani F, Wieckowski MR, et al (2007) Protein kinase C beta and prolyl isomerase 1 regulate mitochondrial effects of the life-span determinant p66Shc. Science **315:** 659–663

Puppo A, Groten K, Bastian F, Carzaniga R, Soussi M, Lucas MM, de Felipe MR, Harrison J, Vanacker H, Foyer CH (2005) Legume nodule senescence: roles for redox and hormone signalling in the orchestration of the natural aging process. New Phytol **165:** 683–701

Rahfeld JU, Rucknagel KP, Schelbert B, Ludwig B, Hacker J, Mann K, Fischer G (1994) Confirmation of the existence of a third family among peptidyl-prolyl cis/trans isomerases: amino acid sequence and recombinant production of parvulin. FEBS Lett **352:** 180–184

Ramirez P, Toledo H, Guiliani N, Jerez CA (2002) An exported rhodanese-like protein is induced during growth of *Acidithiobacillus ferrooxidans* in metal sulfides and different sulfur compounds. Appl Environ Microbiol **68:** 1837–1845

Ranganathan R, Lu KP, Hunter T, Noel JP (1997) Structural and functional analysis of the mitotic rotamase Pin1 suggests substrate recognition is phosphorylation dependent. Cell **89:** 875–886

Reimer T, Weiwad M, Schierhorn A, Ruecknagel PK, Rahfeld JU, Bayer P, Fischer G (2003) Phosphorylation of the N-terminal domain regulates subcellular localization and DNA binding properties of the peptidyl-prolyl *cis/trans* isomerase *h*Par14. J Mol Biol **330:** 955–966

Sali A, Blundell TL (1993) Comparative protein modelling by satisfaction of spatial restraints. J Mol Biol **234:** 779–815

Sekerina E, Rahfeld JU, Muller J, Fanghanel J, Rascher C, Fischer G, Bayer P (2000) NMR solution structure of *h*Par14 reveals similarity to the peptidyl prolyl *cis/trans* isomerase domain of the mitotic regulator *h*Pin1 but indicates a different functionality of the protein. J Mol Biol **301:** 1003–1017

Shi JY, Blundell TL, Mizuguchi K (2001) FUGUE: sequence-structure homology recognition using environment-specific substitution tables and structure-dependent gap penalties. J Mol Biol **310:** 243–257

Shilov IV, Seymour SL, Patel AA, Loboda A, Tang WH, Keating SP, Hunter CL, Nuwaysir LM, Schaeffer DA (2008) The paragon algorithm: a next generation search engine that uses sequence temperature values and feature probabilities to identify peptides from tandem mass spectra. Mol Cell Proteomics **6:** 1638–1655

Simon-Rosin U, Wood C, Udvardi MK (2003) Molecular and cellular characterisation of *Lj*AMT2; 1, an ammonium transporter from the model legume *Lotus japonicus*. Plant Mol Biol **51:** 99–108

Sippl MJ (1993) Recognition of errors in 3-dimensional structures of proteins. Proteins **17:** 355–362

Sudol M (1996) Structure and function of the WW domain. Prog Biophys Mol Biol **65:** 113–132

Surmacz TA, Bayer E, Rahfeld JU, Fischer G, Bayer P (2002) The N-terminal basic domain of human parvulin *h*Par14 is responsible for the entry to the nucleus and high-affinity DNA-binding. J Mol Biol **321:** 235–247

Sylvester DM, Sander C (1990) Immunohistochemical localization of rhodanese. Histochem J **22:** 197–200

Tamura K, Dudley J, Nei M, Kumar S (2007) MEGA4: Molecular Evolutionary Genetics Analysis (MEGA) software version 4.0. Mol Biol Evol **24:** 1596–1599

Tian Q, Nagpal P, Reed JW (2003) Regulation of Arabidopsis SHY2/IAA3 protein turnover. Plant J **36:** 643–651

Uchida T, Fujimori F, Tradler T, Fischer G, Rahfeld JU (1999) Identification and characterization of a 14 kDa human protein as a novel parvulin-like peptidyl prolyl *cis/trans* isomerase. FEBS Lett **446:** 278–282

Westley J (1981) Thiosulfate: cyanide sulfurtransferase (rhodanese). Methods Enzymol **77:** 285–291

Yaffe MB, Schutkowski M, Shen M, Zhou XZ, Stukenberg PT, Rahfeld JU, Xu J, Kuang J, Kirschner MW, Fischer G, et al (1997) Sequence-specific and phosphorylation-dependent proline isomerization: a potential mitotic regulatory mechanism. Science **278:** 1957–1960

Yao JL, Kops O, Lu PJ, Lu KP (2001) Functional conservation of phosphorylation-specific prolyl isomerases in plants. J Biol Chem **276:** 13517–13523

Zhang Y, Daum S, Wildemann D, Zhou XZ, Verdecia MA, Bowman ME, Lucke C, Hunter T, Lu KP, Fischer G, et al (2007) Structural basis for high-affinity peptide inhibition of human Pin1. ACS Chem Biol **2:** 320–328

Zheng H, You H, Zhou XZ, Murray SA, Uchida T, Wulf G, Gu L, Tang X, Lu KP, Xiao ZX (2002) The prolyl isomerase Pin1 is a regulator of p53 in genotoxic response. Nature **419:** 849–853

Zhou XZ, Kops O, Werner A, Lu PJ, Shen M, Stoller G, Kullertz G, Stark M, Fischer G, Lu KP (2000) Pin1-dependent prolyl isomerization regulates dephosphorylation of Cdc25C and tau proteins. Mol Cell **6:** 873–883